Vol. 40, No. 4 (2018) 552-564, DOI: 10.24874/ti.2018.40.04.04

Tribology in Industry

www.tribology.rs

RESEARCH

Electrochemical Investigation of Erosion-corrosion Behavior of 6061 Aluminum Alloy in Marine Environment

M. Lavanya[a], V.R. Murthy[a], P. Rao[b]

[a] *Department of Biotechnology, Manipal Institute of Technology, Manipal Academy of Higher Education, Karnataka, India,*
[b] *Department of Chemistry, Manipal Institute of Technology, Manipal Academy of Higher Education, Karnataka, India.*

Keywords:

Erosion corrosion
Jet impingement
Potentiodynamic polarization
electrochemical impedance spectroscopy
Sea water

Corresponding author:

Padmalatha Rao
Department of Chemistry,
Manipal Institute of Technology,
Manipal Academy of Higher
Education, Karnataka, India.
E-mail: padmalatha.rao@manipal.edu

A B S T R A C T

The liquid-solid erosion-corrosion behavior of aluminum in artificial seawater medium at open circuit has been investigated using a submerged jet impingement rig. The aluminum alloy 6061 coupons subjected to erosion corrosion condition were placed normal to the impinging jet. The gap maintained between the nozzle and the specimen was 5mm. In the present study, sea sand was used as an erodent. Erosion corrosion rate was measured using potentiodynamic polarization and electrochemical impedance spectroscopy methods. At a flowrate of 4 lpm passivation was observed in the potentiodynamic polarization plot which was confirmed by the appearance of inductive loop in the Nyquist plot. At higher flowrates no such condition was observed. The system response to impedance studies was characterized by a high frequency capacitive loop and a capacitive loop at the lower frequency. Surface morphology was studied with scanning electron microscopy (semi quantitative analysis) and atomic force microscopy techniques. Elemental mapping was done with electron dispersive X-ray studies. The erosion-corrosion rate increased with increase in the flow rate and temperature. The results of this work will aid in the selection of material for controlled or reduced material loss in sea water circulating equipment' and pipelines.

1. INTRODUCTION

In industry pipeline networks are considered as arteries and veins of modern civilization. The pipeline networks are implemented in fluid transmission and cooling purposes [1]. Pipeline network finds wide applications in the field of oil and gas industries. The necessity and monitoring of these pipelines arises from the fact that these networks suffer from erosion corrosion which may cause catastrophic failures leading to grave environmental impacts. Erosion–corrosion is a form of tribo-corrosion material loss mechanism caused by flowing fluid (with or without solid particles) damaging the surface layer (passive film) and the parent metal. In fact, studies on erosion-corrosion are receiving the attention of many researchers. Numerous industries are

affected by erosion which includes mining and the pneumatic transportation of solids. Chemical, oil and gas, marine and power generation plants are affected primarily by corrosion and oxidation whereas erosion effects are least. Erosion and corrosion either alone or in combination lead to worst case scenarios.

In reality, mechanical factors may be contributing to the removal of corroded scallops from the surface and flow out in the process fluid moving at high velocity. Pipeline failures due to single-phase or wet-steam erosion-corrosion have caused major failures, resulting in casualties or loss of life as well as extensive plant shut down. In a variety of industrial plants, erosion and erosion-corrosion are the problems that can cause a significant increase in the maintenance and operating cost [2]. Managing corrosion and erosion-corrosion related problems and safety considerations demand huge investment in the industries [3]. On February 9, 2006, in Kakrapar Atomic Power Station unit-2, steam was released in the boiler room due to the rupture of a pipe segment in the 10 % feed line, immediately downstream of flow element as a consequence of erosion-corrosion. In another reported instance, an increase in about 20 % pressure due to a steam valve closure failed a 90° elbow in 18-inch feed water line at the United States Nuclear Regulatory Commission (USNRC) on December 9, 1986. A section of pipe blew out. The pipe was moved about six feet due to the reaction forces. 8 employees present in the area died out of severe burns. Failure analysis revealed the cause to be thinning of the pipe due to single-phase erosion-corrosion [6]. On March 16, 1985, with Haddam Neck operating at 100 percent power an incidence of pipe rupture occurred due to the direct flow impingement on the pipe surface causing a severe erosion of the pipe.

Feed water piping system experienced wall thinning at the Trojan Nuclear Power Plant (1987). The thinning was to such an extent that the pipe wall thickness would have reached the minimum thickness as prescribed by the design code (ANSI - American National Standard Institute (ANSI) Standard B31.7, "Nuclear Power Piping"). As per ASME - American Society of Mechanical Engineers' Boiler and Pressure Vessel Code, these portions were in safety-related areas. The primary mechanism for pipe wall thinning at the pump discharge elbow was found to be erosion/corrosion coupled with cavitation caused by severe flow conditions [7].
In oil and gas producing wells, a significant percentage of corrosion-related failures are constituted through erosion-corrosion by virtue of the high fluid velocities, particles entrained in the system and corrosive environment. 9 % of the corrosion related failures in the oil and gas industry are attributable to erosion-corrosion as reported by Kermani and Harrop [8]. The role of chloride ion and dissolved oxygen in the electrochemical component of flow-induced corrosion of Al-Mg alloy in NaCl solution was assessed by Jafarzadeh et al. Under the flow conditions, the cathodic reaction was not influenced by the increase in the chloride ion concentration but the anodic reaction rate was significantly influenced [9]. Burstien et al investigated the slurry erosion-corrosion behavior of aluminum using a modified slurry erosion rig in aqueous silica slurry. The erosion rates of aluminum in a water slurry were found to be much lower than 0.5 M NaCl and acidic slurries under the same experimental conditions [10]. The effect of surface roughness on the corrosion behavior of low carbon steel in 4 M hydrochloric acid was investigated under laminar and turbulent flowing conditions in the presence of an inhibitor. In both the laminar and turbulent flow regimes with an increase in surface roughness, the corrosion rate increased [11]. Laboratory experiments were carried out to study the corrosion behavior of stainless steels and Ni-base and Co-base alloys at elevated temperature (up to 60 °C) and a high velocity impinging flow. Experiments demonstrated the premature breakdown of passivity facilitated by increased temperature. The passivity breakdown potential was shifted to more active values as a consequence of high velocity impinging flow [12].

Erosion–corrosion performance of Al was investigated at three pH values in an impinging jet apparatus. The results revealed that the response of Al depended on the pH [13]. The erosion-corrosion response was dominated by dissolution at pH 13. Nevertheless, the response differed due to the adherent passive film formed on Al at pH 4 and 7 [14].

Erosion corrosion rate of 3003 Al alloy was studied through an impingement jet system in

ethylene glycol- water solution. The erosion-corrosion rate increased with an increase in the fluid velocity. The effect of fluid impingement angle on Al alloy erosion corrosion was found to be dependent on the competitive effects of the normal and the shear stress [15]. Study of dry sand impact erosion on the mild steel was performed by Naz et al. They concluded that the higher velocities of the solution, containing coarse sand, induce higher plastic deformation on the metal surface. The surface damages can appreciably be reduced by controlling the velocity of the erodent sand as per the findings. [16]. Erosion-corrosion study of X-52 steel pipe under turbulent swirling impinging jets was conducted by Sedano-de la Rosa et al. They found that the swirling regime is more severe than the non-swirling condition, and the maximum corrosion rate was at high swirl numbers. The swirling flow condition enhanced the pit formation, promoting the dissolution of the underlying metal [17]. Erosion-corrosion performance of API steels was studied by Md. Aminul Islam. Corrosion lead to a significant increase in erosion throughout the process significant increase in erosion was observed due to corrosion. Corrosion caused an increase in surface roughness, removal of work hardened layer and accelerated embedded particle removal. It further promotes delamination by extending sub-surface cracks. Likewise, corrosion was also significantly increased due to erosion. Erosion caused removal of corrosion film on the surface, breakage in the cementite network, offered positive conditions for pitting and increased the effective surface area by increasing the surface roughness [18].

The current study investigates the behavior of 6061 aluminum alloy erosion-corrosion conditions with variations in parameters such as flow rate and temperature in a submerged jet impingement rig. A constant sand concentration (0.3 %) was maintained for all experiments.

2. EXPERIMENTAL

2.1 Apparatus

The experiments were carried out in a submerged jet-impingement rig as illustrated in Fig. 1. The experimental rig consisted of a reservoir tank, a pump, flow rate controller, temperature controller, thermocouple, and valves. An electrochemical cell was incorporated into the rig to perform the electrochemical studies.

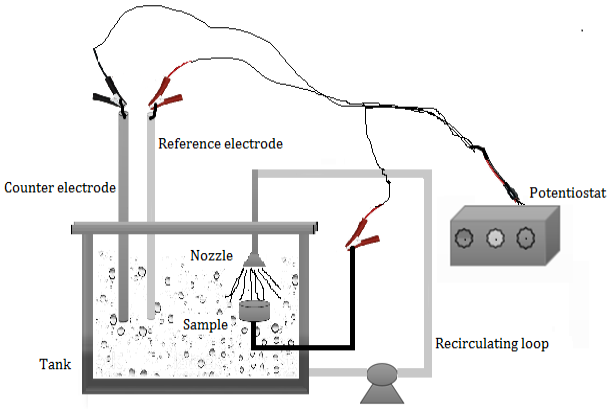

Fig. 1. Experimental rig for erosion corrosion studies.

The slurry was driven by a centrifugal pump through a recirculating loop which leaves the 8 mm diameter nozzle to impact in a direction normal to the specimen. The distance between the nozzle and the specimen was maintained as 5 mm.

2.2 Materials

The electrode for electrochemical studies was made of 6061 aluminum alloy. The composition of it is given in Table 1.

Table 1. Elemental composition of 6061 Al alloy.

Elements	Mg	Si	Cu	Cr	Fe	Al
Composition (%wt)	0.96	0.80	0.27	0.21	0.40	balance

The machined specimens were embedded in epoxy resin leaving a working area of 1.1 cm^2. The circular surface of the electrode was polished using emery papers of sizes ranging from 600 to 1200. It was then disc polished with levigated alumina to obtain a mirror polish.

The testing solution, the artificial seawater was prepared as per ASTM standards (D1141-98). [19]. The composition of artificial water - Sodium Chloride – 58.49 %, Magnesium Chloride - 26.46 %, Sodium Sulfate – 9.75 %, Calcium Chloride – 2.76 %, Potassium Chloride – 1.64 %, Sodium Bicarbonate – 0.47 %, Potassium Bromide – 0.23 %, Boric Acid - 0.07 %, Strontium Chloride – 0.09 %, Sodium Fluoride -0.007 %.

The suspended solids in the slurry were sea sand of size 300 μ. Through out the experiments 0.3 % sand concentration was maintained. For all tests angle of impingement was 90°. Experiments were conducted at temperatures of 303 K, 313 K and 323 K with various flowrates of 4 lpm, 8 lpm, and 12 lpm. The impact velocity V was determined by using the cross-section area of the outlet nozzle, as in equation (1).

$$V_{jet} = Q/A \quad (1)$$

Q is the volumetric flow rate of slurry (m^3s^{-1}) and A is the cross-section area of the outlet nozzle (m^2). The particle velocity is assumed to be that of the jet velocity as given by equation (1) [20].

2.3 Electrochemical measurements

Electrochemical studies were performed by using electrochemical workstation (CH-600 D-Series US model CH instrument, with a beta software on a test cell with three electrodes. A platinum electrode was used as an auxiliary electrode, saturated calomel electrode (SCE) as a reference electrode and aluminum alloy 6061 being the working electrode.

Open circuit potential was determined by immersing the working electrode under the experimental condition for 900 secs. The electrode potential that is measured with respect to the reference electrode when no current flows through it is known as the OCP [21]. Potentiodynamic polarization studies were performed by polarising the electrode ±500 mV at the scan rate of 1mv/ sec. Electrochemical Impedance Spectroscopy studies were conducted with a sinusoidal potential excitation of ± 10 mV amplitude. The frequency range for measurement was chosen from 10 kHz to 10 mHz. PDP studies were performed immediately after impedance studies without surface treatment. The experiment was performed by varying the flow rate of slurry (4 lpm, 8 lpm, and 12 lpm) at varying temperature in the range of 303 K to 323 K. The liquid jet impinged on the specimen at an angle of 90 ° from a nozzle whose exit diameter was 8 mm. The gap of 5 mm was maintained between the nozzle and the specimen. All the studies were repeated with minimum of 3-4 trails and the average of best three agreeing values were reported.

2.4 Surface characterization

Surface morphology studies were carried out using analytical scanning electron microscope (JEOL JSM-6380L). For the same specimen, elemental mapping was done using energy dispersive X-Ray analysis technique. The surface roughness of the specimen was analyzed by AFM technique (IB342 Innova model).

3. RESULTS AND DISCUSSION

Figures 2a, 2b and 2c shows polarization curves measured for aluminum alloy as a function of flow rate of the slurry at a temperature of 303 K, 313 K, and 323 K respectively.

The corrosion rates and Ecorr were evaluated from the polarisation plots using a Tafel extrapolation method which permits the interpretation of experimental data [22].

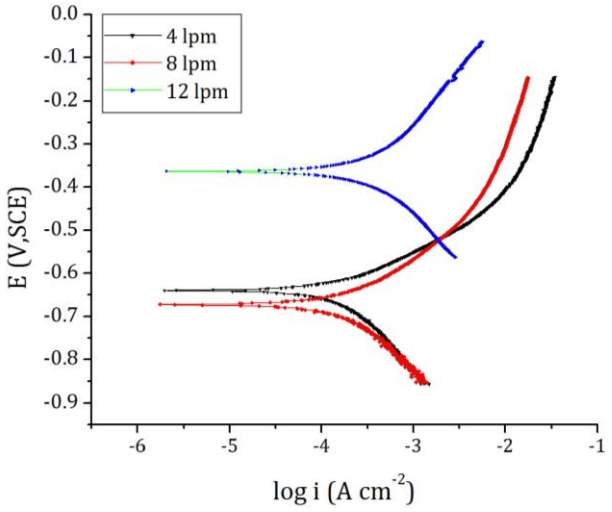

a)

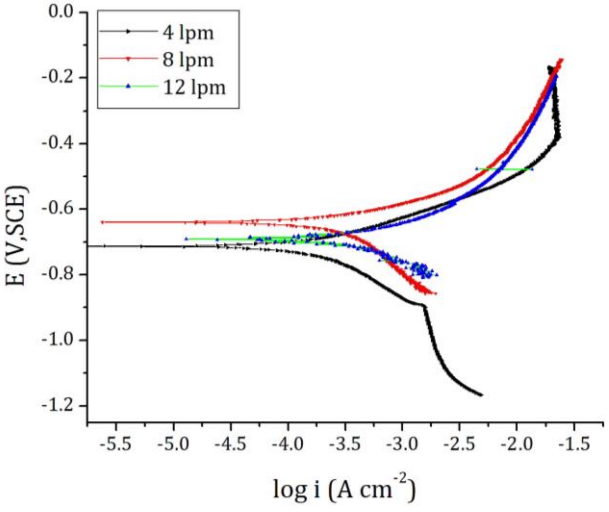

b)

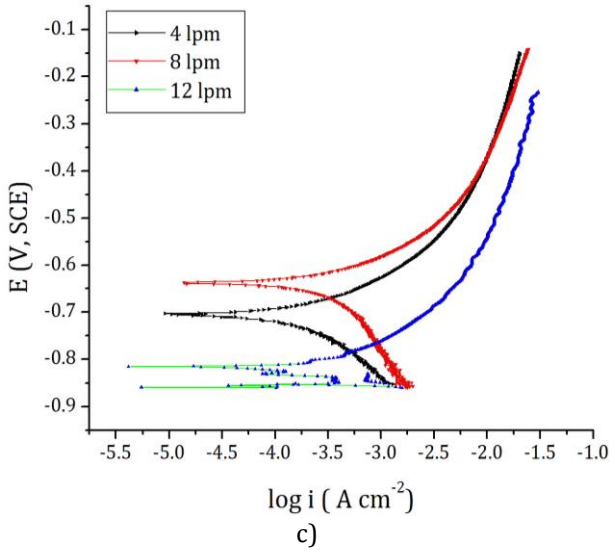

Fig. 2. Potentiodynamic polarisation plots at a) 303 K, b) 313 K and c) 323 K.

The total reduction and oxidation current densities will be equal at the point where the cathodic line for the hydrogen evolution intersects the anodic line for metal dissolution reaction. The potential at which these lines intersect is known as the corrosion potential [23].

In the Fig. 2b, it can be observed that cathodic reaction is accelerated. The acceleration of cathodic reaction could be ascribed to the higher transfer rate of dissolved oxygen [22]. Increase in the flow rate will increase the oxygen availability (increased mass transfer of the cathodic reactant) and thus increase the corrosion rate [24]. Furthermore, under dynamic situations, the corrosion products were easily detached by the flowing fluid, which further accelerated the anodic reaction as observed in Fig. 2a by promoting the metal substrate Al dissolve into metallic ion Al^{3+} [25].

It could be observed that the corrosion rate increased with increase in the flowrate as observed in Table 2. Similar results were also obtained by other research groups [25,26]. As compared to 8 lpm electrode was more active at 12 lpm (Fig. 2c). With the increase in the flow rate, oxygen reduction reaction increased (increase in the cathodic current density) and the mechanical impact of the sand present in the solution was also significantly enhanced. Hence a competition exists between activation and oxidation of electrode in the slurry. Due to sand impingement and dominating activation effect, a negative shift in E_{corr} and a rise in the anodic current density are observed. The increase in i_{corr} indicates a increase in the overall corrosion rate. Passivity is observed only at a flow rate of 4 lpm and disappears at higher flowrates confirming dissolution (Fig. 2b). In case of a passive metal, the rise in flow rate accelerates the removal rate of the passive film, thereby accelerating the overall erosion–corrosion process [27].

At higher impingement velocities the particles impingement velocities increase and extra energy is provided to the moving particles, thus causing more degradation on the specimen surface [28]. In the solutions containing sand concentration less than 0.5 % the increase in the anodic current density is low. Therefore at concentrations below 0.5 %, the electrode surface is not seriously damaged and hence results in significant increase in corrosion rate [15].

Figure 3 depicts the polarization plot of 8 lpm at a different temperature. As observed in Table 2 corrosion rate increases with an increase in the temperature. This result is in consistency with other publications [29,30]. Also corrosion potential (E_{corr}) shifted positively with increase in the temperature.

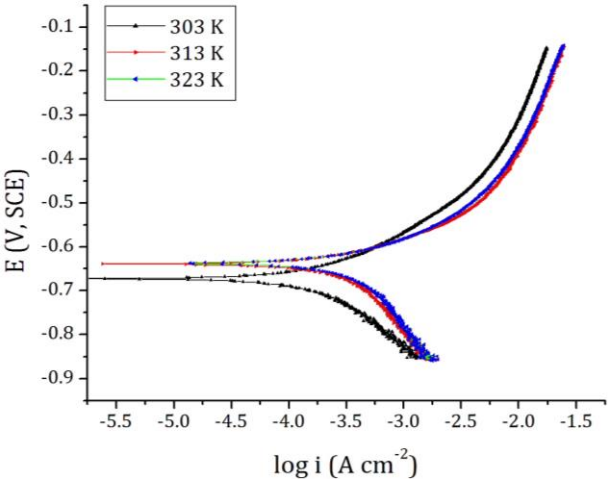

Fig. 3. Potentiodynamic plots at 8 lpm.

From the Table 2, it could be observed that at higher flowrates, current density in general increases as a consequence of the increase in the metal and slurry interaction causing corrosion product removal and active metal dissolution [31]. Depassivation and repassivation kinetics are extremely quick and hence the liquid-solid impinging stream, through the action of continuous impacts and associated repassivation signatures, gives rise to a fluctuating current [32].

Table 2. Results of PDP studies for various temperatures and flowrates (FR).

T	FR	E_{corr}	i_{corr}	βa	-βc	CR
(K)	(lpm)	(mV)	(μA cm^{-2})	(mVdec^{-1})	(mV dec^{-1})	(mmy^{-1})
303	4	-0.64	179.4	943.4	522.5	1.80
	8	-0.672	200.1	742.1	550.4	2.01
	12	-0.363	402.3	493.8	535.9	4.04
313	4	-0.713	208.1	907.1	494.2	2.09
	8	-0.639	397.5	854.0	362.4	3.99
	12	-0.691	613.5	597.1	574.0	6.16
323	4	-0.703	236.5	770.4	588.5	2.58
	8	-0.602	503.3	751.5	345.4	5.04
	12	-0.725	901.6	681.3	246.2	9.06

Electrochemical impedance spectroscopy Nyquist plots for corrosion of AA 6061 at different temperatures are shown in figure 4-6. From the impedance plots semicircles can be observed which indicates that the corrosion process is charge transfer controlled [33].

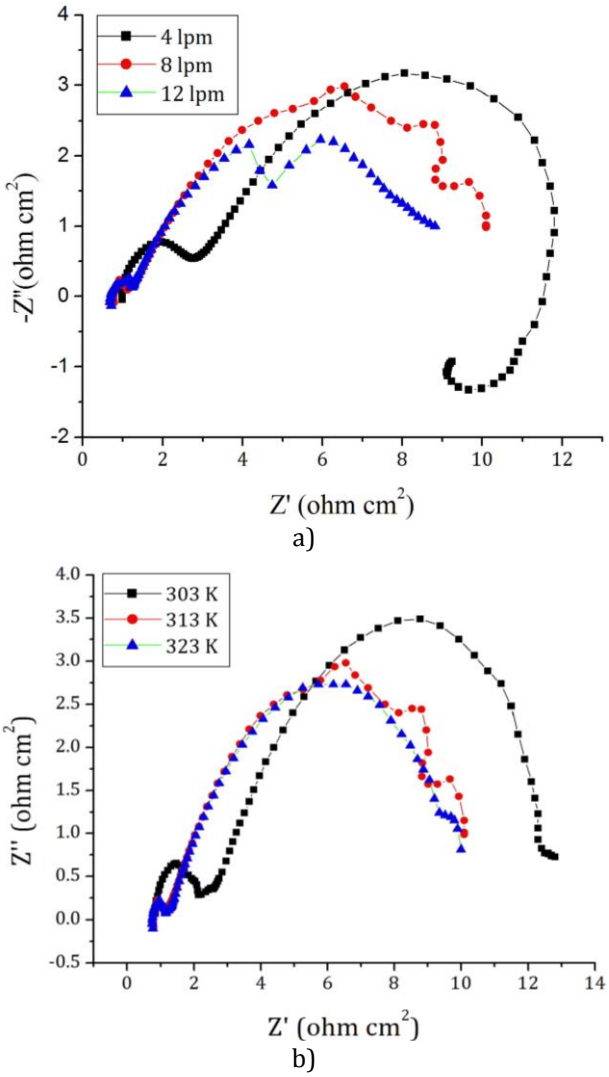

Fig. 4. Nyquist plots at a) 313 K and b) 8 lpm.

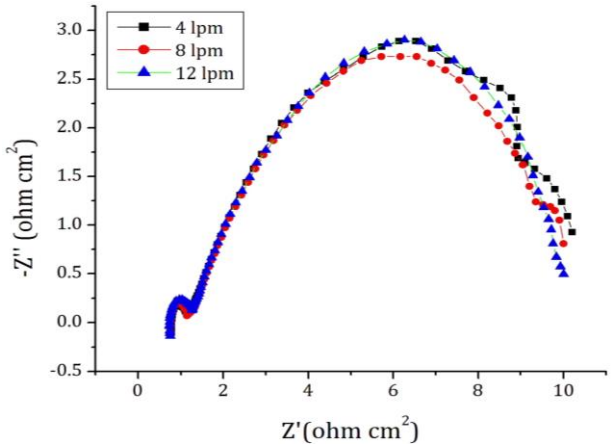

Fig. 5. Nyquist plots for 323 K.

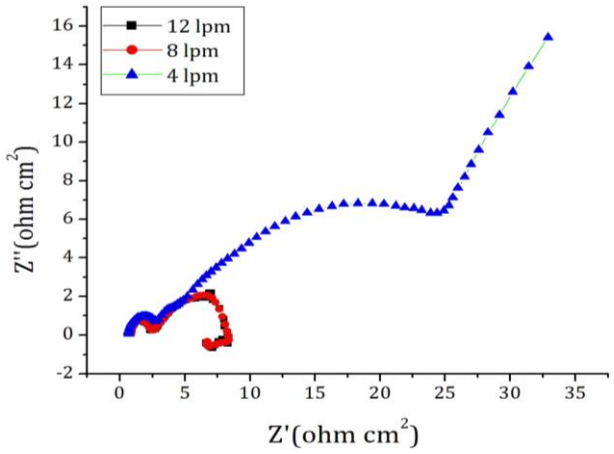

Fig. 6. Nyquist plot for 303 K.

A common feature observed in the Figs. 4-6 is the appearance of two capacitive loops, one in the HF region and the other in the LF region. The capacitive loop is corresponding to the interfacial reactions according to Bret [34]. The high frequency capacitive loop is usually attributed to the charge transfer process of aluminum dissolution reaction and could be accounted for the charge transfer reaction during the corrosion process occurring at the metal/oxide/electrolyte interface. The charge transfer occurs through the formation of Al^{3+}, OH^- and O_2^- at the metal/surface film/electrolyte interface [35].

The capacitive loop at the lower frequency region could be due to the diffusion of ions or electrolyte ingress though the corrosion product/inhibitor layer [36].

The inductive loop that appears in the LF region is ascribed to the surface relaxation process which is a consequence of enhanced surface roughness. Though other explanations for the

appearance of inductive loop include surface activation adsorption [15], in the current study, no typical adsorption is expected. In figure 6 at the low frequency region a straight line with slope close to 45° is observed which is known as the Warburg diffusive impedance [37]. This is attributed to the ionic diffusion of a part of the corrosion product through the oxide layer on the alloy surface [38]. The data obtained from impedance is analysed through equivalent circuits. Figures 7-10 shows the simulated circuit for the experimentally obtained Nyquist plots.

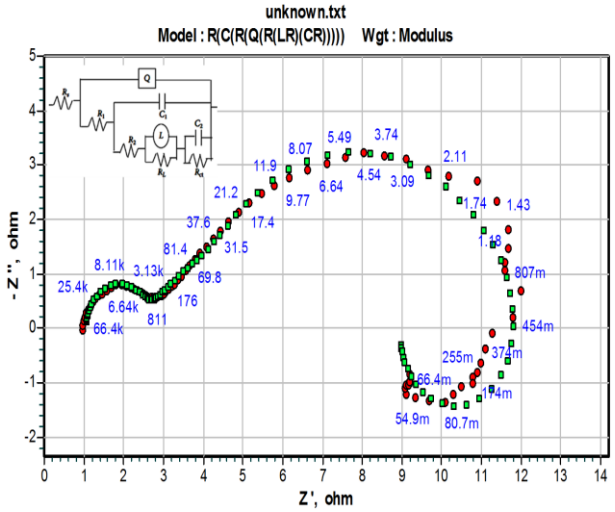

Fig. 7. Simulated circuit fit to the obtained EIS data.

The equivalent circuit in Fig. 7 was found to be the best fit for the experimental results shown in Fig. 4a (4 lpm).The nine elements of the circuit in Fig. 7 are solution resistance R_S, charge transfer resistance (R_{ct}), inductive resistance (R_L), the metal/oxide resistance R_1, oxide/solution resistance R_2, inductive element (L), a constant phase element, Q , capacitors C_1 and C_2. The five-element equivalent circuit as shown in Fig. 8 was found to be the best fit for the experimental results shown in Figs. 4-6. The elements of the circuit are solution resistance (R_S), film resistance (R_1), charge transfer resistance R_{ct}. time constant of the electrical double layer (CPE_1), the capacitance of the surface film (CPE_2). The equivalent circuit in Fig. 9 included eight elements. Namely, the solution resistance (R_S), the capacitance C_1 and C_2, resistances, a constant phase element Q, R_1, R_2, R_{ct} and the warburg element W. The details of the circuit elements are shown in Fig. 10 [39]. Capacitance and the resistance values obtained were from circuit fitment. The double layer capacitance (C_{dl}) and polarization resistance (R_p) are calculated in accordance with the Eqs. (2)-(5) and the calculated electrochemical parameters obtained from circuit fitment along with the goodness of fit are given in Table 3.

$$C_{dl}=1/2\Pi f_{max}R_p \quad (2)$$

$$R_p= R_1+R_2+R_L+R_{ct} \quad (3)$$

$$R_p=R_1+R_{ct} \quad (4)$$

$$R_p=R_1+R_2+R_{ct} \quad (5)$$

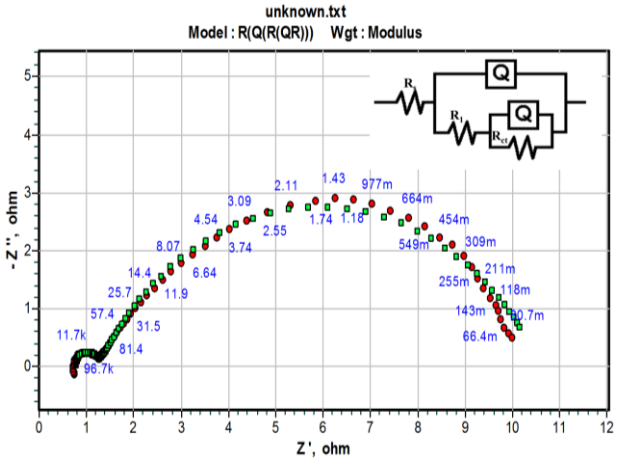

Fig. 8. Simulated circuit fit to the obtained EIS data.

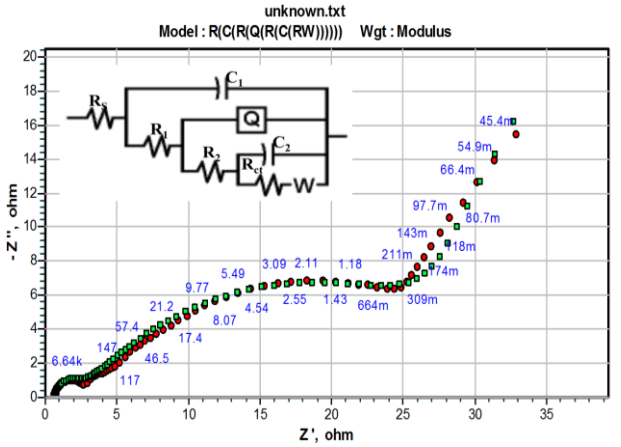

Fig. 9. Simulated circuit fit to the obtained EIS data.

Equation (2) is used to calculate capacitance for all the simulated circuits. Whereas Equation (3), (4) and (5) are used for the calculation of Rp for the simulated circuits in Figs. 7-9 respectively. Bode plot analysis is simple as compared to Nyquist plot. Bode diagram gives a clear explanation of how the electrochemical system behaves depending upon the frequency and how it reduces the experimental data dispersion. Extrapolation and analysis of the impedance data at LF could be most conveniently performed using Bode plot. Figure 11 display the

plots of Bode magnitude. From the plot, the R_p values can be obtained from the difference between HF limit and LF limit in Bode plots. These differences in decreased with increase in temperature and impingement velocity as well as presented by other researchers [25].

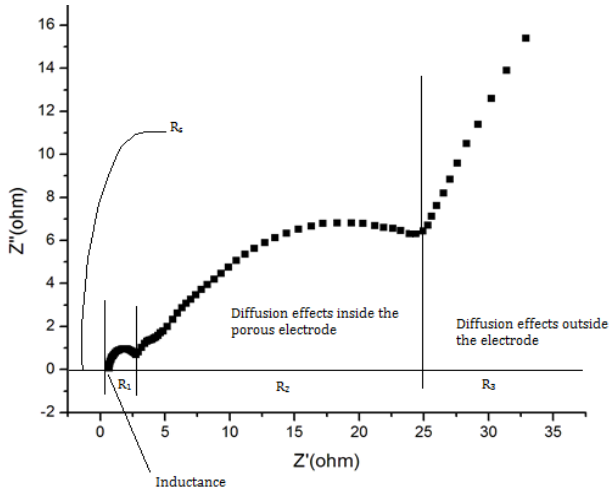

Fig. 10. Nyquist plot details for simulated circuit.

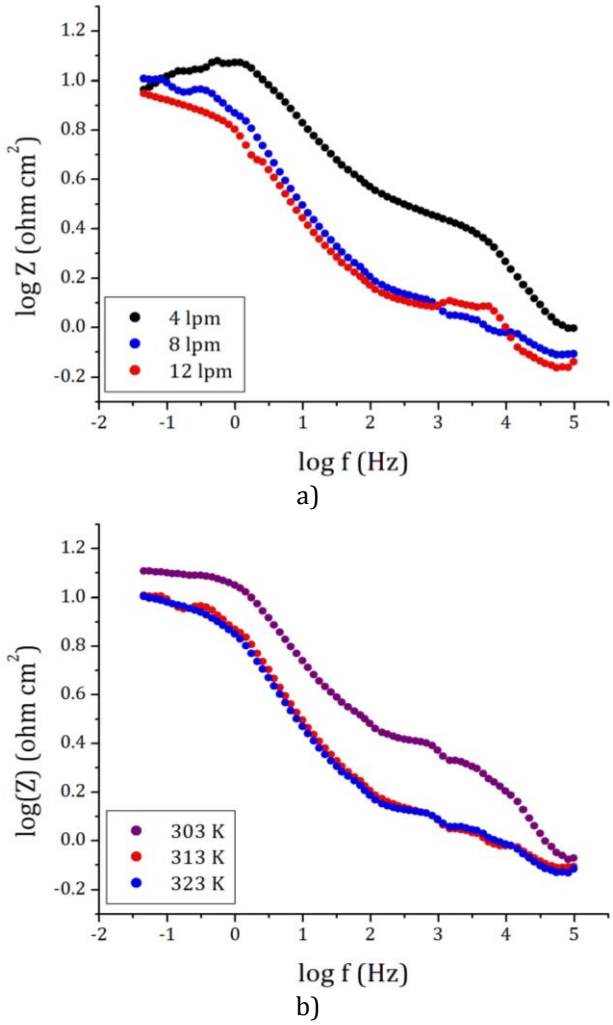

Fig. 11. Bode magnitude plot at: a) 313 K and b) 8 lpm.

Figures 11a and 11b discloses that impedance value is larger 4 lpm when compared with 8 and 12 lpm and also it is larger for 303 K in comparison with 313 and 323 K respectively; this observation is ascribed to low corrosion rate at 4 lpm and 313 K. Results in the Table 3 indicate decrease in resistance and C_{dl} shows a positive trend indicating an increase in the corrosion rate with increase in flowrate.

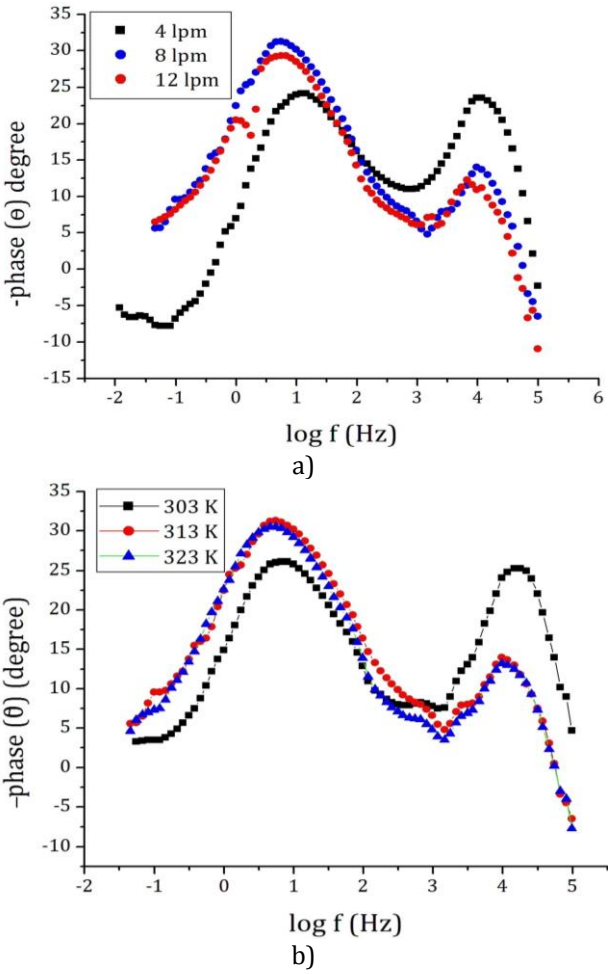

Fig. 12. Bode phase plot at: a) 313 K and b) 8 lpm.

EDX, SEM micrographs of the sand before and after the test are shown. Figures 13-14 shows the morphology of sand before and after the experimental run. There was not much change observed in the surface roughness and sharpness of the sand particles. Hence, concluding that the sand was not degraded during the course of the experiment. Figure 15 shows the formation of pits, deep craters and indentations whereas platelets and lips formation is minimal. One of the explanations may be that under E-C conditions for Al alloy 6061, electrochemical corrosion mechanism dominates over mechanical erosion process.

Table 3. Results of EIS studies for various temperatures and flowrates (FR).

T (K)	303			313			323		
FR (lpm)	4	8	12	4	8	12	4	8	12
R_p (Ω cm^2)	75.57	19.93	8.7	17.683	10.15	8.7417	10.17	9.848	9.83
C_{dl} (μF cm^{-2})	6.00*10-4	6.57*10-4	8.87*10-3	2.79*10-3	5.67*10-3	9.33*10-3	2.74*10-3	5.74*10-3	5.76*10-3
$\chi 2$ ($\times 10^{-3}$)	4.554	2.123	2.510	1.834	2.541	5.139	2.047	2.678	3.217

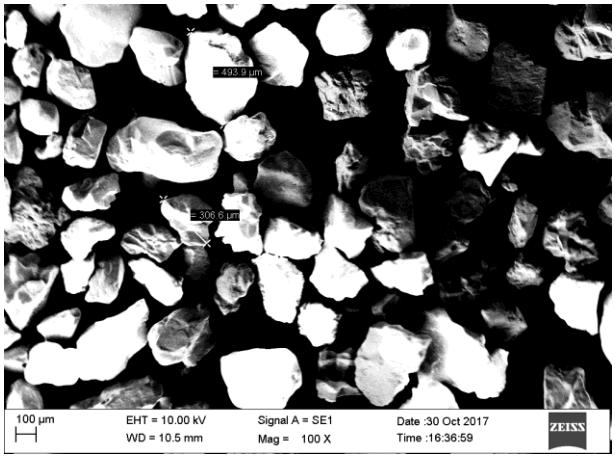

a)

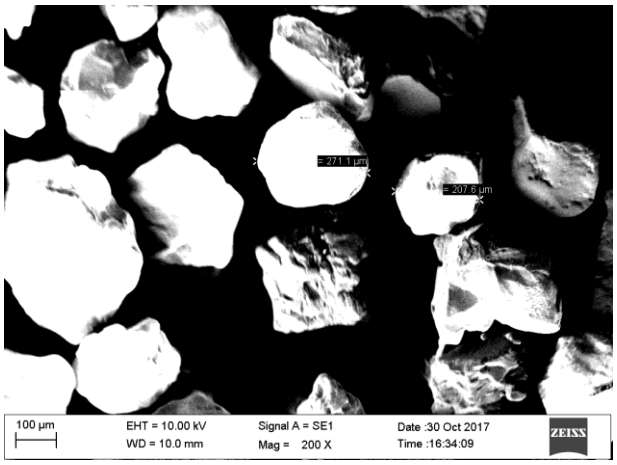

b)

Fig. 13. SEM images of sand particles before impingement test a) 100x and b) 200x.

Corrosion attacks the weakened layer at the eroded surface thus exposing the indented area. Hutchings found that erosion of ductile metals at normal incidence occurs by delamination. According to literature, at high impact angles brittle materials fracture whereas heavy plastic deformation is experienced by the surface of ductile materials [40]. The corrosion pits have a large size of about 100 µm. The erosion pits formed by the microjet impacts have sizes of a few micrometers. The corrosion pit is characterized by the formation of corrosion products inside and around the pit. It has a large size and is shallow which is characterized by traces of particle removal. The erosion pit has a small size of about 10 µm or less. [41] When the sample is placed at an angle 90̊ to the impinging fluid minimum damage due to shear force is caused by the erodent particles in the slurry and hence there is negligible metal loss can be expected due to abrasion [42].

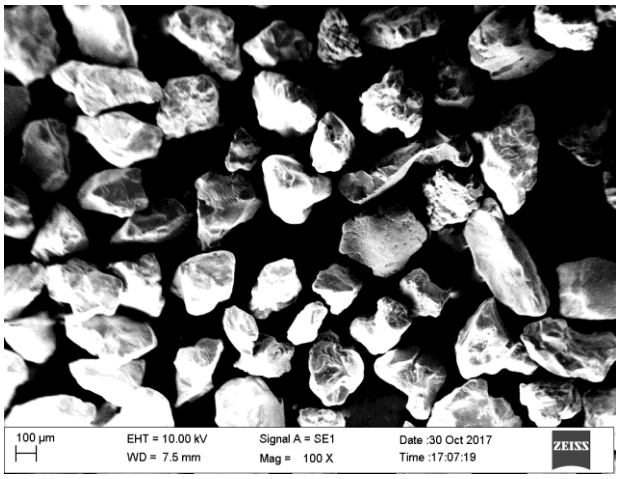

a)

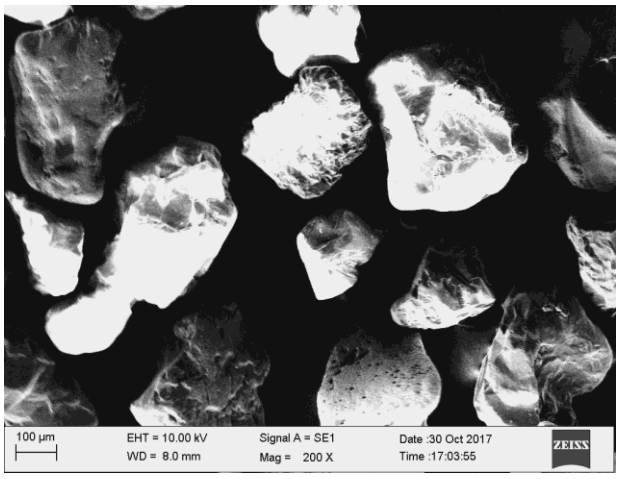

b)

Fig. 14. SEM images of sand particles after impingement test a) 100x and b) 200x.

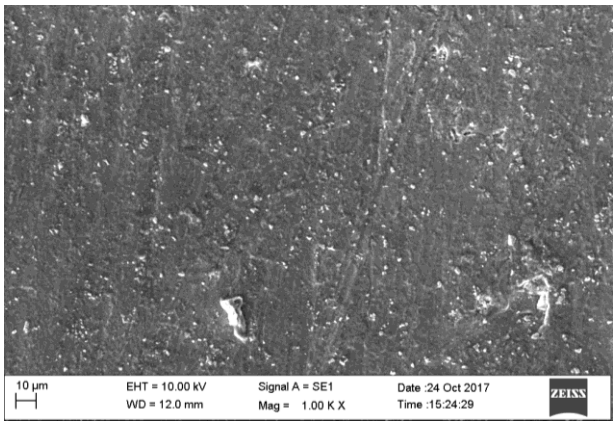

a)

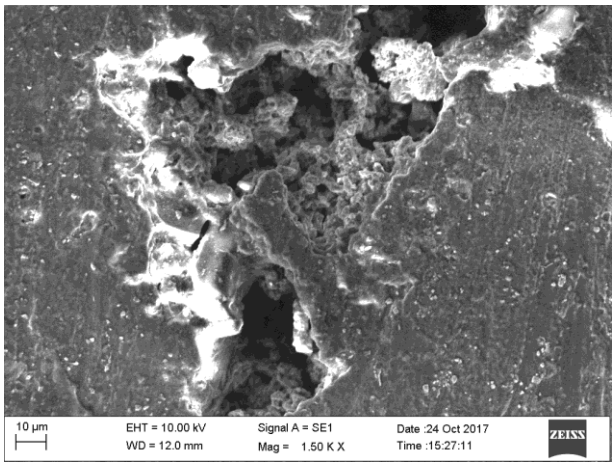

b)

Fig. 15. SEM images of the Al alloy surface showing the deep craters caused by E-C at a magnification of a) 1000x and b) 1500x.

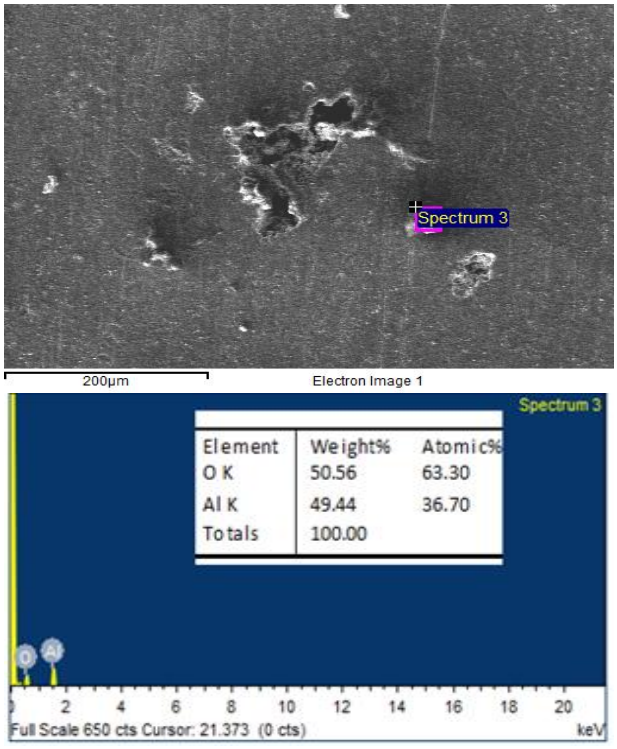

Fig. 16. EDX analysis of the eroded metal surface at 8 lpm.

Further pit formation in this area is due to subsequent corrosion attack [25]. The successive impact of the particles in the slurry causes enhanced surface roughness. From the data of the worn out surface as shown in Fig. 16 the presence of aluminum and oxygen is observed. Aluminum is a part of the base metal composition whereas oxygen is not. The chemical compositions in weight % for the alloy obtained under energy-dispersive X-ray spectroscopy (EDS) were examined.

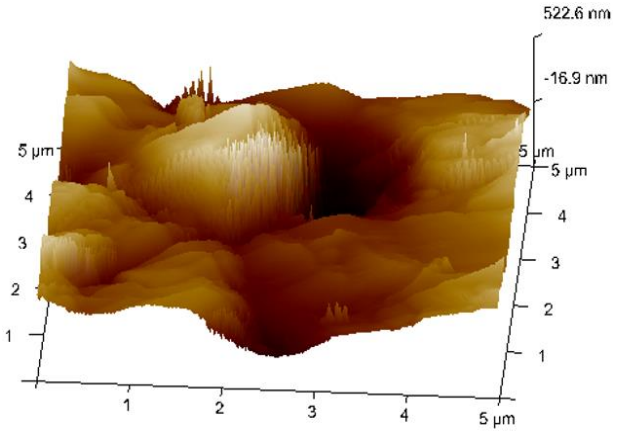

Fig. 17. AFM image of Al alloy surface at 8 lpm.

The decrease in aluminum content (49.44 %) and oxygen (50.56 %) shows the metal degradation [32]. Figure 17 shows a 3-dimensional image of AFM at 8 lpm. At higher flowrates sample indentation caused by the sand particle impingement is visible. Deeper indentation leads to a greater chance of failure.

4. CONCLUSION

The E–C behavior of the 6061 aluminum alloy was investigated with a submerged jet impingement rig. Following conclusions are drawn from the study.

- Passivation film on the surface of 6061 aluminum alloy was observed at 4 lpm which disappeared with increase in the slurry flow rate indicating low durability of the protective layer.
- Erosion corrosion rate of 6061 aluminum alloy increased with increase in the slurry flow rate and temperature.
- EIS studies showed that there was a decrease in the overall resistance with the increase in the flowrates.

- Impedance studies exhibited the presence of two capacitive loops.
- The low frequency capacitive loop directs the growth of surface film which further results in increased polarization resistance.
- The results obtained will assist in selecting the optimum flowrate and temperature for slurry transportation and thus aid in increasing the lifespan of the pipeline.
- The data obtained from the jet impingement rig will thus help in determining the optimum slurry flow conditions.

Acknowledgement

The authors would like to acknowledge Department of Biotechnology and Department of Chemistry MIT, Manipal for extending the laboratory facilities.

Abbreviations

PDP - Potentiodynamic polarization

EIS - Electrochemical Impedance Spectroscopy

E-C - Erosion corrosion

lpm - Liter per minute

CPE - Constant Phase Element

HF - High frequency

LF - Low frequency

REFERENCES

[1] W. Zhao, C. Wang, T. Zhang, M. Yang, B. Han, A. Neville, *Effects of laser surface melting on erosion–corrosion of X65 steel in liquid–solid jet impingement conditions*, Wear, vol. 362-363, pp. 39-52, 2016, doi: 10.1016/j.wear.2016.05.006

[2] J. H. Tylczak, *Erosion–corrosion of iron and nickel alloys at elevated temperature in a combustion gas environment,* Wear, vol. 302, iss. 1-2 pp. 1633-1641, 2013, doi: 10.1016/j.wear.2013.01.008

[3] X. Hu, R. Barker, A. Neville, A. Gnanavelu, *Case study on erosion–corrosion degradation of pipework located on an offshore oil and gas facility*, Wear, vol. 271, iss. 9-10, pp. 1295-1301, 2011, doi: 10.1016/j.wear.2011.01.036

[4] V. Kain, *Flow accelerated corrosion: forms, mechanisms and case studies*, Procedia Engineering, vol. 86, pp. 576-588, 2014, doi: 10.1016/j.proeng.2014.11.083

[5] M.M. Muhammadu, J. Sheriff, E. Hamzah, *Review of literature for the flow accelerated corrosion of mitred bends*, International Journal of Emerging Technology and Advanced Engineering, vol. 3, iss. 8, pp. 663-677, 2013.

[6] H.S. Bush, *The Effects of Erosion-Corrosion on Power Plant Piping*, in Proceeding of The 59th General Meeting of The National Board of Boiler and Pressure Vessel Inspectors, Tennessee, Nashville, 1990.

[7] P.C. Wu, *Erosion/Corrosion-Induced Pipe Wall Thinning in US Nuclear Power Plants*, Nuclear Regulatory Commission, no. NUREG-1344, Washington, United States, 1989.

[8] S. Tandon, M. Gao, R. McNealy, *Erosion-corrosion failure of a carbon steel pipe elbow-a case study*, in Corrosion 2009, 22-26 March, 2009, Atlanta, Georgia, NACE International, pp. 4531-4543.

[9] K. Jafarzadeh, T. Shahrabi, S.M.M. Hadavi, M.G. Hosseini, *Role of chloride ion and dissolved oxygen in electrochemical corrosion of AA5083-H321 aluminum-magnesium alloy in NaCl,* Journal of materials science and technology, vol. 23, iss. 5 , pp. 623-628, 2007.

[10] Y. Li, G.T. Burstein, I.M. Hutchings, *The influence of corrosion on the erosion of aluminium by aqueous silica slurries*, Wear, vol. 186-187, pp. 515-522, 1995, doi: 10.1016/0043-1648(95)07181-4

[11] B. Evgeny, T. Hughes, D. Eskin, *Effect of surface roughness on corrosion behaviour of low carbon steel in inhibited 4M hydrochloric acid under laminar and turbulent flow conditions*, Corrosion Science, vol. 103 pp. 196-205,2016, doi: 10.1016/j.corsci.2015.11.019

[12] A. Neville, T. Hodgkiess, *An assessment of the corrosion behaviour of high-grade alloys in seawater at elevated temperature and under a high velocity impinging flow*, Corrosion Science vol. 38, iss. 6, pp. 927-956, 1996, doi: 10.1016/0010-938X(96)00180-1

[13] L.Y. Xu, Y.F. Cheng, *Electrochemical characterization and CFD simulation of flow-assisted corrosion of aluminum alloy in ethylene glycol–water solution*, Corrosion Science, vol. 50, iss. 7, pp. 2094-2100 2008, doi: 10.1016/j.corsci.2008.05.004

[14] M. M. Stack, N. Pungwiwat, *Particulate erosion–corrosion of Al in aqueous conditions: some perspectives on pH effects on the erosion–corrosion map*, Tribology International, vol. 35, iss. 10, pp. 651-660, 2002, doi: 10.1016/S0301-679X(02)00056-7

[15] G.A. Zhang, L.Y. Xu, Y. F. Cheng, *Investigation of erosion–corrosion of 3003 aluminum alloy in ethylene glycol–water solution by impingement jet system*, Corrosion science, vol. 51, iss. 2, pp. 283-290, 2009, doi: 10.1016/j.corsci.2008.10.026

[16] M.Y. Naz, S.A. Sulaiman, S. Shukrullah, A. Ghaffar, K.A. Ibrahim, N.M. AbdEl-Salam, *Development of erosion-corrosion mechanisms for the study of steel surface behavior in a sand slurry*, Measurement, vol. 106, pp. 203-210, 2017, doi: 10.1016/j.measurement.2017.04.042

[17] C. Sedano-de la Rosa, M. Vite-Torres, J.G. Godínez-Salcedo, E.A Gallardo-Hernández, R. Cuamatzi-Melendez, L.I. Farfán-Cabrera, *Erosion-corrosion of X-52 steel pipe under turbulent swirling impinging jets*, Wear, vol. 376-377, pp. 549-556, 2017, doi: 10.1016/j.wear.2016.12.063

[18] M.A. Islam, Z. Farhat, *Erosion-corrosion mechanism and comparison of erosion-corrosion performance of API steels*, Wear, vol. 376-377, pp. 533-541, 2017, doi: 10.1016/j.wear.2016.12.058

[19] ASTM D1141-98, *Standard Practice for the Preparation of Substitute Ocean Water,* 2013.

[20] R.J.K. Wood, *The sand erosion performance of coatings,* Materials & design, vol. 20, iss. 4, pp. 179-191, 1999, doi: 10.1016/S0261-3069(99)00024-2

[21] J.A. Beavers, *Corrosion of steel piling in nonmarine applications*, National Academy Press, 1998.

[22] G.A. Zhang, Y.F. Cheng, *Electrochemical corrosion of X65 pipe steel in oil/water emulsion*, Corrosion Science, vol. 51, iss. 4, pp. 901-907, 2009, doi: 10.1016/j.corsci.2009.01.020

[23] G.S. Frankel, *Fundamentals of corrosion kinetics*, in A. Hughes, J. Mol, M. Zheludkevich, R. Buchheit (Ed.): Active Protective Coatings, Springer Series in Materials Science, vol. 233, pp. 17-32, 2016, doi: 10.1007/978-94-017-7540-3_2

[24] R.C. Barik, J.A. Wharton, R.J.K. Wood, K.S. Tan, K.R. Stokes, *Erosion and erosion–corrosion performance of cast and thermally sprayed nickel–aluminium bronze*, Wear, vol. 259, iss. 1-6, pp. 230-242, 2005, doi: 10.1016/j.wear.2005.02.033

[25] Z.B. Zheng, Y.G. Zheng, *Erosion-enhanced corrosion of stainless steel and carbon steel measured electrochemically under liquid and slurry impingement*, Corrosion Science, vol. 102 pp. 259-268, 2016, doi: 10.1016/j.corsci.2015.10.014

[26] Q. Zheng, L. Zhang , X. Jie , X. Huang , S. Luo, *Effect of Rotating Speed and Hydrostatic Pressure on Erosion-Corrosion Behavior of X65 Pipeline Steel*, International Journal of Electrochemical Science, vol. 12, pp. 2593-2605, 2017, doi: 10.20964/2017.03.10

[27] S.S. Rajahram, T.J. Harvey, R.J.K. Wood, *Erosion–corrosion resistance of engineering materials in various test conditions*, Wear, vol. 267, iss. 1-4, pp. 244-254, 2009, doi: 10.1016/j.wear.2009.01.052

[28] H. Meng, X. Hu, A. Neville, *A systematic erosion–corrosion study of two stainless steels in marine conditions via experimental design*, Wear, vol. 263, iss. 1-6, pp. 355-362, 2007, doi: 10.1016/j.wear.2006.12.007

[29] B.W. Madsen, *Measurement of erosion-corrosion synergism with a slurry wear test apparatus*, Wear, vol. 123, iss. 2 pp. 127-142, 1988, doi: 10.1016/0043-1648(88)90095-6

[30] A. Neville, T. Hodgkiess, *Study of effect of liquid corrosivity in liquid-solid impingement on cast iron and austenitic stainless steel*, British Corrosion Journal, vol. 32, iss. 3, pp. 197-205, 1997.

[31] S.B. Choe, S.J. Lee, *Effect of flow rate on electrochemical characteristics of marine material under seawater environment*, Ocean Engineering, vol. 141, pp. 18-24, 2017, doi: 10.1016/j.oceaneng.2017.05.035

[32] A. Neville, M. Reyes, H. Xu, *Examining corrosion effects and corrosion/erosion interactions on metallic materials in aqueous slurries*, Tribology International, vol. 35, iss. 10, pp. 643-650, 2002, doi: 10.1016/S0301-679X(02)00055-5

[33] P.R. Kumari, J. Nayak, A.N. Shetty, *Corrosion behavior of 6061/Al-15 vol. pct. SiC (p) composite and the base alloy in sodium hydroxide solution,* Arabian Journal of Chemistry, vol. 9, pp. s1144-s1154, 2016, doi: 10.1016/j.arabjc.2011.12.003

[34] C.M.A. Brett, *The application of electrochemical impedance techniques to aluminium corrosion in acidic chloride solution*, Journal of applied electrochemistry, vol. 20, iss. 6, pp. 1000-1003, 1990, doi: 10.1007/BF01019579

[35] J. Bessone, C. Mayer, K. Jüttner, W.J. Lorenz, *AC-impedance measurements on aluminium barrier type oxide films*, Electrochemica Acta, vol. 28, iss. 2, pp.171-175, 1983, doi: 10.1016/0013-4686(83)85105-6

[36] K. Zhang, W. Yang, B. Xu, Y. Chen, X. Yin, Y. Liu, H. Zuo, *Inhibitory effect of konjac glucomanan on pitting corrosion of AA5052 aluminium alloy in NaCl solution*, Journal of colloid and interface science, vol. 517, pp. 52-60, 2018, doi: 10.1016/j.jcis.2018.01.092

[37] C. Zhong, X. Tang, Y. F. Cheng, *Corrosion of steel under the defected coating studied by localized electrochemical impedance spectroscopy*,

Electrochimica Acta, vol. 53, iss. 14, pp. 4740-4747, 2008, doi: 10.1016/j.electacta.2008.02.014

[38] N. Dinodi, A.N. Shetty, *Alkyl carboxylates as efficient and green inhibitors of magnesium alloy ZE41 corrosion in aqueous salt solution*, Corrosion Science, vol. 85, pp. 411-427, 2014, doi: 10.1016/j.corsci.2014.04.052

[39] C. Aksakal, A. Sisman, *On the Compatibility of Electric Equivalent Circuit Models for Enhanced Flooded Lead Acid Batteries Based on Electrochemical Impedance Spectroscopy*, Energies, vol. 11, iss. 1, pp. 1-14, 2018, doi: 10.3390/en11010118

[40] B.G. Prakashaiah, D.V. Kumara, A.A. Pandith, A.N. Shetty, B.E.A. Rani, *Corrosion inhibition of 2024-T3 aluminum alloy in 3.5% NaCl by thiosemicarbazone derivative*, Corrosion Science, vol. 136, 2018, doi: 10.1016/j.corsci.2018.03.021

[41] M.A. Islam, Z.N. Farhat, *Effect of impact angle and velocity on erosion of API X42 pipeline steel under high abrasive feed rate*, Wear, vol. 311, iss. 1-2, pp. 180-190, 2014, doi: 10.1016/j.wear.2014.01.005

[42] S. Das, Y.L. Sarawathi, D.P. Mondal, *Erosive corrosive wear of aluminium alloy composites: Influence of slurry concentration and speed*, Wear, vol. 261, iss. 2, pp. 180-190, 2006, doi: 10.1016/j.wear.2005.09.013